PNAS RESEARCH ARTICLE | PHYSICS

Scale invariance in early embryonic development

Miloš Nikolić[a,b], Victoria Antonetti[a,c], Feng Liu[b,d], Gentian Muhaxheri[a,c], Mariela D. Petkova[e], Martin Scheeler[a], Eric M. Smith[a], William Bialek[a,b,f,1], and Thomas Gregor[a,b,g,1]

Affiliations are included on p. 10.

Contributed by William Bialek; received February 15, 2024; accepted October 1, 2024; reviewed by Susan E. Lott, Rob Phillips, John Reinitz, and Pieter Rein ten Wolde

The expression of a few key genes determines the body plan of the fruit fly. We show that the spatial expression patterns for several of these genes scale precisely with embryo size. Discrete positional markers such as the peaks in striped patterns or the boundaries of expression domains have positions along the embryo's major axis proportional to embryo length, accurate to within 1%. Further, the information (in bits) that graded patterns of expression provide about a cell's position can be decomposed into information about fractional or scaled position and information about absolute position or embryo length; all information available is about scaled position, with <2% error. These findings imply that the underlying genetic network's behavior exhibits scale invariance in a more precise mathematical sense. We argue that models that can explain this scale invariance also have a "zero mode" in the dynamics of gene expression, and this connects to observations on the spatial correlation of fluctuations in expression levels.

genetic networks | embryonic development | pattern formation | scaling

Significance

The dimensions of macroscopic patterns, from the branching of snowflakes to the rippling of sand dunes, are determined by the properties of their component parts. As such, larger versions of those systems typically have more repetitions of the same basic pattern elements. Living organisms are different: Larger organisms have the same numbers of pattern elements but these scale in size, so that proportions remain the same. We show that scaling is visible in the fruit fly's first few hours of embryonic development. It is exact: >98% of the information cells have about their position in the embryo is in scaled coordinates. This near-perfect scaling strongly constrains the dynamics of the underlying genetic networks.

Closely related organisms can vary widely in size, but variations in their proportions are much smaller (1–4). A precise mathematical statement of this qualitative observation would be more stringent: The linear dimensions of all elements in the body plan are proportional to the linear dimensions of the organism. If such a precise relationship exists, could it also be present and detectable in the embryo during early development when the body plan first emerges?

Many living systems exhibit "allometric scaling," power-law relationships among different quantities across a well-defined class of organisms (5–7). In some cases, these relations connect the linear dimensions of different body parts. Nonetheless, exact spatial scaling in embryonic development—conforming to the mathematical definition below (Eq. **1**)—would be quite surprising, as it would mean that a truly scale-invariant body plan is determined early and perhaps maintained throughout the many complex stages of development.

The exploration of complex pattern formation in nature dates back centuries (8). Today, we understand the mechanisms of pattern formation in a wide range of nonbiological systems, from fluid flows to crystal growth (snowflakes) and more (9–13) but none of these examples generate patterns that are invariant to the system size in the sense that we consider here. Instead, the pattern elements have linear dimensions set by microscopic parameters, and larger systems exhibit more repetitions of the same pattern rather than expansion or contraction of pattern elements to match the size of the system as a whole (14).

In living systems, genetic networks similarly determine patterning at the molecular level. The pioneering work of Turing (15) on this topic has been extended in many later models (16–18). Still, the basic structure of Turing's original equations for biochemical networks is closely related to models of the inanimate pattern formation. If we take these analogies literally, we would predict that taller people should have more vertebrae, which is obviously wrong. Can a given genetic mechanism succeed in tying the length scales of molecular events to the macroscopic scale of the body plan?

Here, we use the first few hours of development in the fruit fly as an example where we can define and test a precise notion of scale invariance along the anterior–posterior (AP) axis. We focus on protein concentrations as the functional output of the relevant genetic networks and follow the flow of information about a cell's position as it flows through three layers of the network, from maternally deposited morphogens to the gap genes to the pair-rule genes (19–21).

In the spirit of earlier work (22–26), we start by analyzing discrete positional markers, such as the stripes in pair rule-gene expression, and find that their positions vary in

Author contributions: W.B. and T.G. designed research; M.N., V.A., F.L., G.M., M.D.P., M.S., E.M.S., W.B., and T.G. performed research; W.B. contributed new reagents/analytic tools; M.N., V.A., G.M., M.D.P., E.M.S., W.B., and T.G. analyzed data; and M.N., W.B., and T.G. wrote the paper.

Reviewers: S.E.L., University of California Davis; R.P., California Institute of Technology; J.R., The University of Chicago; and P.R.t.W., FOM Institute for Atomic and Molecular Physics (AMOLF).

The authors declare no competing interest.

[1]To whom correspondence may be addressed. Email: wbialek@princeton.edu or tg2@princeton.edu.

This article contains supporting information online at https://www.pnas.org/lookup/suppl/doi:10.1073/pnas.2403265121/-/DCSupplemental.

Published November 8, 2024.

proportion to the length of the embryo with better than 1% accuracy (27). We then take a more general approach, decomposing the information carried by graded patterns of gap gene expression into information about the absolute position x along the AP axis and information about fractional or scaled position x/L, where L is the length of the embryo. All available information is about scaled position along the AP axis, with <2% errors.

These results provide strong evidence for scaling in a precise mathematical sense for both the gap genes and the pair-rule genes. But at least one of the maternally deposited morphogens, Bicoid (Bcd) (28, 29), does not show any sign of scale invariance within genetically uniform populations (1, 22, 30). As in well-understood, nonbiological pattern-forming systems, models of the Bcd profile have a length scale λ set by the underlying molecular parameters (protein diffusion and degradation); in this picture, the spatial profile of concentration $C_{\rm Bcd}(x) \sim \exp(-x/\lambda)$, and the question of scaling is whether $\lambda \propto L$. Here, using the more general information-theoretic approach, independent of the functional form, we find that Bcd expression does not scale with the embryo length. Taken together, our results suggest that scaling in the gap genes is an emergent property of the network, and it seems natural to assume that scaling in the pair-rule genes is inherited from their gap gene inputs.

Even though scale invariance is a statement about spatial properties of the gene expression patterns, we argue theoretically that true scale invariance places specific requirements on network dynamics, independent of molecular details: The network must have a "zero mode." We can decompose the spatial variations of gene expression into modes, analogous to normal modes in a mechanical system, that relax independently as the system approaches its steady state. A zero mode has a zero decay rate, resulting in nonlinear decay even when it is very near the steady state. Zero modes also are easily perturbed by noise, leading to system-wide fluctuations and long-range spatial correlations, as observed experimentally in the embryo (25, 31, 32) and in more detailed models (33, 34).

Testing for Scaling

There is a general idea that the concentrations of particular molecules—morphogens—determine the fates of cells in a developing embryo (35). Since fates are tied to cell positions, morphogen concentrations must carry information about position along the body axes. In the early fly embryo, the identities of all the relevant morphogens are known, and their rich spatial patterns are established before cell membranes form and before cells make large-scale movements (36). This brings the system close to the idealization of molecules diffusing and interacting in a single large container.

We focus on pattern formation along the AP axis. We will analyze measurements of gene expression as a function of absolute position x (in μm) along the AP axis of length L. Multiple morphogen species, indexed by i, have concentration profiles described by continuous functions $g_{\rm i}(x;L)$, assuming we ignore the discreteness of cells. This notation highlights that profiles can vary with embryo size L.

True scale invariance means that the concentration of morphogens depends solely on position relative to the embryo's length, $x_s \equiv x/L$:

$$g_{\rm i}(x;L) = \Phi_{\rm i}(x_s). \qquad [1]$$

If there is a fixed map from morphogen concentrations to cell fates, this scaling behavior would ensure that cells adopt a fate based on their relative position x/L, rather than on x and L separately.

The most straightforward way to test for scale invariance in a pattern is to identify a specific point in the spatial pattern and measure its position as a function of the embryo length L. We emphasize that scale invariance is not just about positional markers adjusting to the embryo length in absolute terms; it requires that this adjustment is exactly linear with zero intercept, as defined in Eq. **1**.

To illustrate, consider a gene expression pattern $g_{\rm i}$ with a single peak along the AP axis, where the peak is at position $x = x_p$. We can then write $g_{\rm i}$ with the origin at x_p:

$$g_{\rm i} = g_{\rm i}(x - x_{\rm p}; L). \qquad [2]$$

Then, scale invariance as defined in Eq. **1** requires

$$g_{\rm i}(x - x_{\rm p}; L) = \Phi_{\rm i}\left(\frac{x - x_p}{L}\right). \qquad [3]$$

To remove all dependence on L we must have

$$x_{\rm p} = \langle f_{\rm p}\rangle \cdot L + \text{noise}, \qquad [4]$$

where f_p is the fractional or scaled peak position, $\langle\cdots\rangle$ denotes the average over many embryos of different lengths, and noise accounts for variation across embryos. This concept extends to concentration profiles with multiple peaks, as seen with the pair-rule genes (Fig. 1 *A* and *B*).

Embryos in an inbred laboratory stock fluctuate in length with a SD of $\sigma_L/\langle L\rangle \sim 4\%$ (37, 38); see also *SI Appendix*, section A. But we know that morphogens in the early fly embryo carry enough information to specify scaled positions with ∼1% precision along the AP axis (39, 40). To reconcile these numbers, it seems that positional signals have to scale with embryo length, but we must be careful.

Imagine a hypothetical embryo where a morphogen profile peak (or another characteristic marker) is perfectly placed at an absolute position x_p relative to the anterior pole. The only source of variation of the measured relative position $f_p \equiv x_p/L$ across a population of such hypothetical embryos is the variation in L. Assuming the position x_p is "anchored" to the anterior (A) of the embryo, as it could be for a nonscaling pattern, the variance of f_p is given by

$$\sigma^2_{f_{\rm p}}(A) \equiv \langle(\delta f_{\rm p})^2\rangle = \langle x_{\rm p}\rangle^2\left[\left\langle\left(\frac{1}{L}\right)^2\right\rangle - \left\langle\frac{1}{L}\right\rangle^2\right]. \qquad [5]$$

Thus, the SD of the relative position $\sigma_{f_{\rm p}}$ depends on the position of the marker x_p relative to the embryo anterior. The fractional error in position is, in first order:

$$\sigma_{f_{\rm p}}(A) \sim \frac{\langle x_{\rm p}\rangle}{\langle L\rangle}\cdot\frac{\sigma_L}{\langle L\rangle}.$$

For a marker that is, on average, a quarter of the way from the anterior to posterior ($\langle x_{\rm p}\rangle = 0.25\langle L\rangle$), fluctuations will be $\sigma_{f_{\rm p}}(A) \sim 0.01$ even without scaling. Similarly, if we have a marker anchored at some fixed absolute position relative to the posterior (P), the variance in relative position will linearly decrease toward the posterior:

$$\sigma_{f_{\rm p}}(P) \sim \left(1 - \frac{\langle x_{\rm p}\rangle}{\langle L\rangle}\right)\cdot\left(\frac{\sigma_L}{\langle L\rangle}\right). \qquad [6]$$

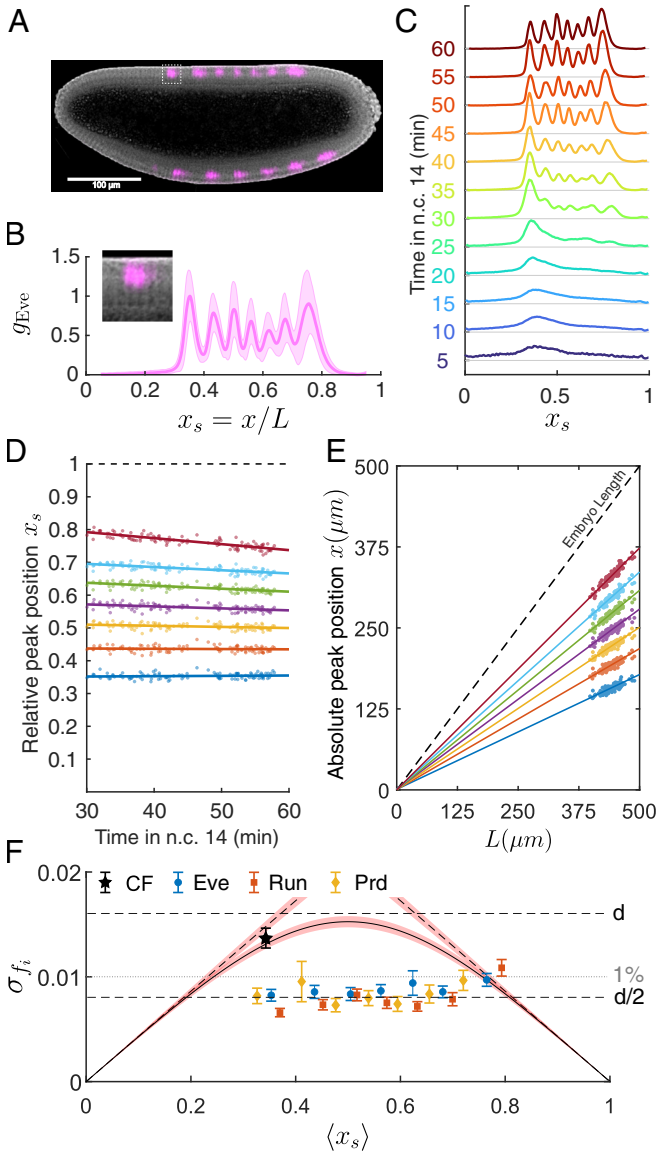

Fig. 1. Precise scaling of pair-rule stripes in the *Drosophila* embryo. (*A*) Bright-field image overlaid with fluorescent antibody staining for Eve protein (fuchsia), focusing on the mid-sagittal plane with the dorsal side up. (Scale bar, 100 μm.) (*B*) Expression of Eve in the second half of nuclear cycle fourteen (nc14). The solid line is the mean, and the shaded region is the SD across $N_{\mathrm{em}} = 108$ embryos in a time window between 30 and 60 min from the start of nc14. The *Inset* shows a single nucleus with a white square (width 0.01 *L*) used to average intensities. (*C*) Eve expression profiles as a function of relative position along the body axis for 12 time bins during nc14, as indicated by color. (*D*) Linear dynamics of Eve peak positions during nc14, fit to Eq. **11**. (*E*) Absolute positions of the dorsal Eve stripes measured at a distance *x* from the anterior pole. There are seven Eve stripes as shown in (*B*). Each point corresponds to a position of the fitted stripe center in one embryo, and stripe order is indicated by color. Absolute positions are corrected for time $t_0 = 45$ min, as in Eq. **12** and as shown in (*D*). (*F*) SD of scaled stripe positions as a function of mean position for three pair-rule genes and for the cephalic furrow (CF; see *SI Appendix*, section C). Error bars for σ_f are estimated from bootstrapping. Black curves with red shading (bootstrapped errors) are estimates of precision based on anchoring in Eqs. **5**–**7**, and *d* is the spacing between neighboring cells.

We can also imagine cells combining anterior and posterior signals to reduce error, resulting in

$$\frac{1}{\sigma^2_{f_{\mathrm{p}}}(A,P)} = \frac{1}{\sigma^2_{f_{\mathrm{p}}}(A)} + \frac{1}{\sigma^2_{f_{\mathrm{p}}}(P)}. \qquad [7]$$

With $\sigma_L/\langle L\rangle \sim 0.04$, fluctuations in relative position could be less than ∼1.4% along the entire AP axis, even without a scaling mechanism. Therefore, convincing ourselves that pattern formation is truly scale invariant requires precise measurements and depends on the system itself operating at high precision.

It is intuitive to think about scaling as the proportionality of a small set of marker positions to embryo length, as in Eq. **4**. However, it should be possible to test the scaling of the entire morphogen profile, as in Eq. **1**, more directly and at each position x_s in the embryo. To achieve this, we need a way to compare expression profiles in embryos of different lengths. Since morphogen profiles are noisy, expecting the exact equality of two functions across all values of x_s is unrealistic. Fortunately, the noise level itself provides a useful metric for comparison. To make this precise we use an information theoretic formulation.

The statement that morphogen profiles depend on x and L means that the concentrations of these molecules provide information about the underlying positional variables. As first shown by Shannon, the intuitive notion of "provide information" has a unique mathematical formulation (41–43). If we write the gene expression levels as $\mathbf{g} \equiv \{g_i\}$ then the information that some particular molecular signals provide about absolute position and embryo length will be $I(\mathbf{g} \to \{x, L\})$. But if we ask about the average of this information over all the possible signals that cells in the embryo can see, this average is symmetric; generally $I(a \to b) = I(b \to a)$, and this is referred to as the mutual information (41–43):

$$I(\mathbf{g};\{x,L\}) = \int d\mathbf{g} \int dx \int dL\, P(\mathbf{g}|\{x;L\}) \times P(x,L) \log_2 \left[\frac{P(\mathbf{g}|\{x,L\})}{P(\mathbf{g})}\right] \text{bits}, \qquad [8]$$

where for more compact notation, we write $d\mathbf{g} = \prod_i dg_i$. The (conditional) distribution $P(\mathbf{g}|\{x, L\})$ is the probability of finding the set of morphogen concentrations $\{g_i\}$ at position x in an embryo of length L; this distribution has a peak near the mean gene expression profile and the width around this peak quantifies the noise in the expression levels. The (marginal) distribution $P(\mathbf{g})$ is the probability of finding these concentrations averaged over all values of x and L; and $P(x, L)$ is the distribution of positions and lengths. This information is mutual because the concentrations of morphogens provide cells with information about position, and specifying position and length allows us to predict the concentrations. Importantly, information depends on both the mean spatial profiles of the morphogens and their noise levels.

True scale invariance means that all of the information conveyed by morphogens is about the scaled position x/L:

$$I(\mathbf{g};\{x,L\}) = I(\mathbf{g};x/L) \quad \text{(perfect scaling)}. \qquad [9]$$

In other words, specifying the scaled position is enough to predict morphogen concentration; no extra information is gained by knowing x and L separately. Conversely, we can separate the total information into two components: the mutual information between the relative position x/L and gene expression $\mathbf{g}$, and an increment that describes the deviation from scaling:

$$I(\mathbf{g};\{x,L\}) = I(\mathbf{g};x/L) + \Delta I, \qquad [10]$$

With samples from a sufficiently large number of embryos, we can make a reliable estimate of ΔI. The smaller the fraction $\Delta I/I(\mathbf{g};x/L)$ the closer the system is to a mathematical ideal of scaling. More explicit expressions for ΔI are developed in *SI Appendix*, section B, and applied to the experiments below.

We emphasize that true scale invariance, corresponding to $\Delta I = 0$, is an extreme condition. Different levels of evidence for scaling in embryonic development have inspired models in which competing mechanisms can provide some cancellation of the intrinsic length scales determined by diffusion constants and reaction rates (44–47). These models typically allow for scaling in the position of a single discrete positional marker (e.g., the middle of the embryo), or for approximate scaling across a larger segment of the relevant axes. True scale invariance would require new dynamical mechanisms.

Stripes and Boundaries

In the early fly embryo, information about position along the AP axis flows from maternal morphogens to the network of gap genes and then to the pair-rule genes (21). The pair-rule genes are expressed in striped patterns that preview the segmented body plan in the fully developed organism; these stripes are visible within three hours after the egg is laid (Fig. 1 *A–C*). The positions of pair-rule stripes are a clear example of the positional markers discussed above.

Here we analyze the spatial profiles of gene expression for three of the pair-rule genes—*eve*, *prd*, and *run*—for which we have a large dataset of precise measurements thanks to the existence of high-quality antibodies (40). Each of these genes fulfills a primary role in establishing the segmented body plan of the fly, each is expressed in seven stripes, and these stripes alternate Prd/Eve/Run over much of the embryo ($0.33 \lesssim x/L \lesssim 0.8$). Gene expression is measured using fluorescent antibody staining of the corresponding proteins in more than one hundred embryos, fixed during nuclear cycle 14 (nc14), i.e., 2 to 3 h after oviposition. These measurements provide snapshots of the protein concentrations in each embryo, and we can mark time in nc14 to ∼1 min precision by measuring the progress of the cellularization membrane (39); this timing precision is crucial in testing for scaling (27).

Pair-rule stripes gradually appear in the second half of nc14. Once visible, it is straightforward to localize the position of each stripe x_i (27, 40). Stripe positions vary systematically (23, 48–51) and are well described by a linear function of time

$$\frac{x_i(t)}{L} = \frac{x_i(t_0)}{L} + s_i(t - t_0), \qquad [11]$$

as shown for the Eve stripes in Fig 1*D*. To compare data from embryos fixed at different times, we adjust stripe position to a reference time $t_0 = 45$ min,

$$\frac{x_i(t_0)}{L} = \frac{x_i(t)}{L} - s_i(t - t_0). \qquad [12]$$

We apply this same procedure to Prd and Run stripes, which appear slightly later in development.

Fig. 1*E* shows that the stripe positions x_i measured from the anterior pole are proportional to the length of the embryo L. More precisely, if we fit these linear relations then intercepts are zero and slopes are equal to the mean scaled positions, as in Eq. **4**, with error bars <1% (*SI Appendix*, section C). This provides prima facie evidence for scaling of the pair-rule stripes, reinforcing the conclusions of earlier work (22–25).

We can go beyond the mean behaviors to look at fluctuations around these means. For each stripe i in each embryo α, we can write

$$\frac{x_i^\alpha}{L^\alpha} = \langle f_i \rangle + \delta f_i^\alpha, \qquad [13]$$

where $\langle \cdots \rangle$ now is an average over all the embryos in our sample. The variance of the relative position is $\sigma_{f_i}^2 = \langle (\delta f_i)^2 \rangle$, and Fig. 1*F* shows that $\sigma_{f_i} \leq 0.01$ for all 21 pair rule stripes that we measure. This is consistent with previous measurements, and with the information content of the gap gene expression patterns that feed into the generation of pair-rule stripes (40, 52), but earlier work did not address scaling explicitly.

As a caution, we note that the observation of scaling in fixed embryos would be trivial if variations in embryo length were dominated by shrinkage during fixation. Across $N_{em} = 609$ fixed embryos used for the analysis of gap genes (below) we find a mean length $\langle L \rangle_{fix} = 455$ μm, while across $N_{em} = 610$ live embryos (below) we find $\langle L \rangle_{live} = 490$ μm. Hence, shrinkage with fixation is a bit less than 10% across many different experiments. But the variations in length are almost the same, $(\sigma_L/\langle L \rangle)_{fix} = 0.038$ vs. $(\sigma_L/\langle L \rangle)_{live} = 0.037$. The small extra variance in the length of fixed embryos cannot explain the scaling behavior that we observe.

Fig. 1*F* also shows that the fluctuations in scaled position are smaller than the bound on mechanisms without explicit scaling. This bound, Eq. **7**, calculated as the error in positioning due to variation in embryo length, is very tight because of the small variance in lengths (black curve with red shading in Fig. 1*F*). Demonstrating that a point in the expression pattern scales requires extreme precision in the measurement and the embryo's functional behavior. Notably, all pair-rule stripe positions scale better than this bound across a broad stretch of the central AP axis.

The importance of precision, both experimental and biological, is clear when contrasting the results from pair-rule genes with the position of the cephalic furrow—a single row of cells marking the end of nc14 and separating the head from the body (36, 53). Our analysis shows that the position of the cephalic furrow, x_{CF}, scales with L as a straight line with zero intercept (*SI Appendix*, section C), and the positioning error of the cephalic furrow is just over 1%, both consistent with the idea that the furrow is determined by pair-rule gene expression (54). Because of experimental constraints in tracking single cell row movements (53), we cannot exclude the possibility that a significant component of this error is measurement error. The result is that the precision of the cephalic furrow measurement is not good enough to provide evidence for scaling, since it is (barely) consistent with the variance that can be reached by mechanisms that do not involve scaling, from Eq. **7**; see the black star in Fig. 1*F*.

The pair-rule stripes are shaped by input from the gap genes (55), and it is natural to ask whether the scaling behavior that we observe is inherited from these inputs. It has been evident for a long time that the gap genes control the pair-rule genes in a dose-dependent manner (56). But we now know that the extent of this control is even more striking: The positional information encoded by the gap genes is optimally decoded by the pair-rule genes (40, 52, 57). As a first step in analyzing the scaling of the gap genes, we use the boundaries of the expression domains as positional markers (Fig. 2 *A–D*) and follow the same ideas as for the pair-rule stripes.

Previous experiments have measured the expression profiles of the gap genes (40), staining $N_{em} = 609$ fixed embryos in nc14 with fluorescent antibodies directed at the proteins encoded by these genes (Fig. 2 *A–D*). We define expression boundaries as the positions where the concentrations are half their maximum value as in ref. 39, and we correct their relative positions to $t_0 = 45$ min as above. Fig. 2*E* shows that all thirteen gap gene boundaries defined in this way have absolute positions that scale

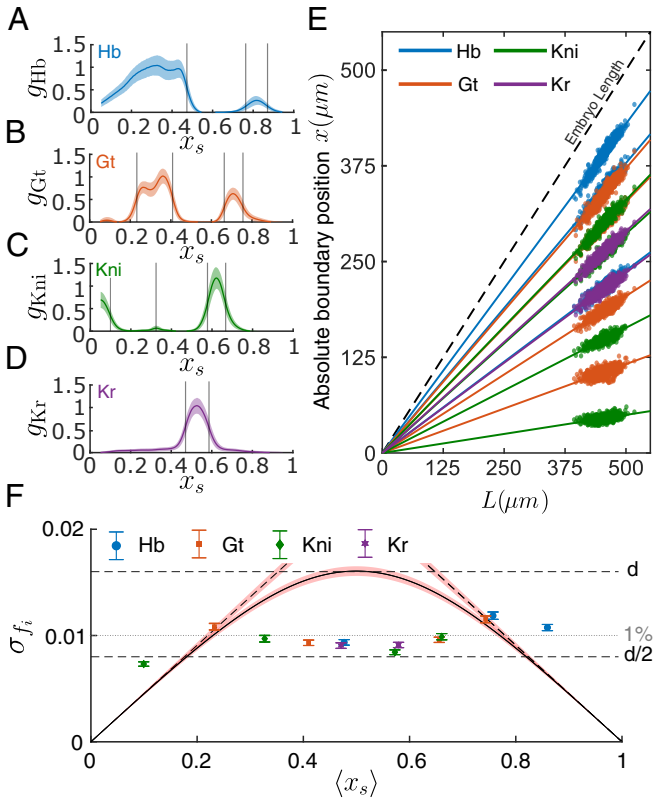

Fig. 2. Precise scaling of gap gene expression boundaries. Expression profiles of (*A*) Hunchback (Hb), (*B*) Giant (Gt), (*C*) Knirps (Kni), and (*D*) Krüppel (Kr), based on immunofluorescent staining (*SI Appendix*, section D). Means (solid lines) and SDs (shading) across embryos aligned by scaled position x_s. Vertical lines indicate the mean positions of expression boundaries and a small peak in Kni. (*E*) Absolute position of all gap gene boundaries as a function of embryo length. Four gap genes are color-coded as shown in the legend. There are multiple expression domain boundaries per each gene as shown in (*A*–*D*), some overlapping. The dashed black line indicates the position of the posterior of the embryo. Boundary positions are time-corrected to $t_0 = 45$ min, as with the stripe positions in Fig. 1*D*. (*F*) SD of scaled boundary positions as a function of mean position for all 13 markers. Error bars for σ_f are estimated from bootstrapping. Black curves with red shading (bootstrapped errors) are estimates of precision based on anchoring in Eqs. **5**–**7**, and d is the spacing between neighboring cells. Horizontal dashed lines denote the distance d and half-distance $d/2$, between neighboring nuclei. The dotted gray line indicates 1% precision.

precisely with embryo length, as with the positions of the pair-rule stripes. The accuracy of this scaling again is better than ∼1%, and this precision is better than the limiting performance of mechanisms that do not have some explicit sensitivity to embryo length (Fig. 2*F*). For the gap genes, this gives more data points, covering almost the entire AP axis ($0.1\,L < x < 0.86\,L$).

In summary, stripes and boundaries of gene expression in the early fly embryo provide discrete positional markers, and the absolute positions of these markers are proportional to the length of the embryo. This is consistent with previous observations (22–25), but the precision of the scaling that we observe here is surprising. This suggests that the underlying genetic network exhibits true scale invariance, which we now test using the information decomposition in Eq. **10**.

Absolute vs. Scaled Positional Information

The concentrations of morphogens provide cells with information about their position in the embryo. This "positional information" (35) can be measured in bits if we have access to data on the mean and variability of spatial profiles for the concentration of the relevant molecules (21). Previous work has shown that the local expression levels of individual gap genes convey roughly two bits of information about position, twice what is possible in a model of on/off expression domains (52, 57). Together the four gap genes provide ∼4.2 bits, sufficient to specify positions with ∼1% accuracy along the AP axis, as seen above. However, these earlier analyses assumed implicitly that information is about the fractional or scaled position. Is this correct?

The key to separating information about scaled vs. absolute position is to compare the variance in morphogen concentrations at a scaled position x_s depending on whether we constrain the length of the embryo as in Eq. **10** (*SI Appendix*, section B). Qualitatively, if there is perfect scaling then fixing the embryo length of all embryos in the population would not add any information with which to predict the morphogen concentration. Since information is mutual this would mean that all the available information is about the scaled position. To test this quantitatively in the context of the gap genes, we have assembled data on $N_{em} = 301$ embryos, in each of which we have reliable simultaneous measurements on the spatial profiles of expression in all four gap genes (*SI Appendix*, section D).

Fig. 3*A* shows the spatial profile of Hb as a function of scaled position along the AP axis. At each scaled position x_s, the distribution of expression levels can be well approximated by

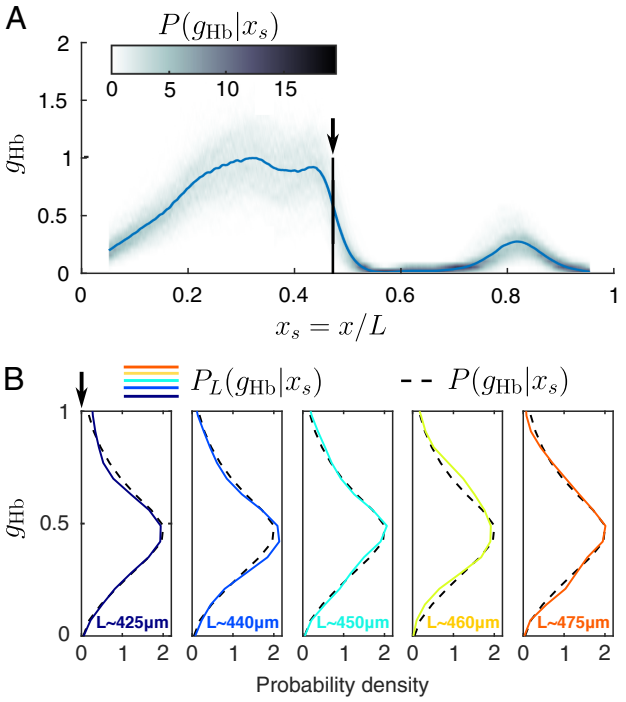

Fig. 3. Expression of Hb in scaled coordinates. (*A*) Mean concentration of Hb, $\langle g_{Hb}(x_s) \rangle$, vs. scaled position (solid line, as in Fig. 2*A*) and the conditional distribution $P(g_{Hb}|x_s)$ around this mean (shading). Intensity bin size is 0.05 maximum $\langle g_{Hb} \rangle$. (*B*) A slice through the conditional distribution at $x_s = 0.47$ (dashed black lines) compared with distributions estimated from embryos in narrow bins of length, $P_L(g_{Hb}|x_s)$ (colored lines). Deviation from scaling would be obvious if the distributions from the subsamples were narrower than the distribution across all embryos. Lengths were binned in 5 bins with an equal number of embryos in each, such that each bin contains about 60 embryos with variations in L of less than 1%. Mean lengths in each bin are indicated at the *Bottom* of each panel. Probability distributions of g_{Hb} are estimated using a kernel density estimator with a Gaussian kernel that has width $\delta g = 0.07 \times \max_{x_s} \langle g_{Hb}(x_s) \rangle$.

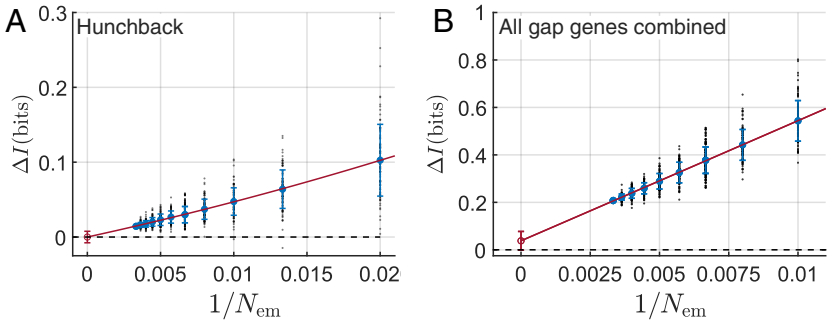

Fig. 4. Near zero deviation from perfect scaling, in bits. (*A*) The extra information ΔI that Hb expression levels carry about absolute rather than scaled position, defined by Eq. **10** and evaluated from Eq. **14**. Estimates are based on random choices of N_{em} embryos out of the full experimental ensemble (points; circles show means with SDs), and the extrapolation $N_{\mathrm{em}} \to \infty$ follows the methods of *SI Appendix*, section E (red line). The result is $\Delta I = 0.00 \pm 0.008$ bits (red circle with error bar). (*B*) The extra information ΔI conveyed by all four gap genes together, defined as in (*A*) by Eq. **10** but now evaluated using Eq. **15**. Symbols as in (*A*); the result is $\Delta I = 0.038 \pm 0.039$ bits. Error bars are larger because we are analyzing a multidimensional code, but there still is no significant difference from $\Delta I = 0$.

a Gaussian (52); an example is the dashed line in Fig. 3*B* (*SI Appendix*, section D). The width of this distribution $P(g_{\mathrm{Hb}}|x_s)$ characterizes the noise in gene expression and sets limits on the information that cells can extract from these expression levels to determine their position and hence their fate. But we can ask what happens if we look only at embryos in a narrow range of lengths around some particular L; Fig. 3*B* shows that all these distributions $P_L(g_{\mathrm{Hb}}|x_s)$ are essentially the same and the same as the full distribution $P(g_{\mathrm{Hb}}|x_s)$. This is a hint that the expression level g_{Hb} is tied to the scaled position $x_s = x/L$ *independent* of the embryo length L, pointing toward precise scaling.

To test for precise scaling we want to estimate ΔI in Eq. **10**, the difference between the total positional information and the information about the scaled position. As explained in *SI Appendix*, section B, this is related to the difference in entropy between the distributions $P_L(g_{\mathrm{Hb}}|x_s)$ and $P(g_{\mathrm{Hb}}|x_s)$. In general, ΔI is difficult to estimate and even more difficult if we include all four gap genes. But things simplify enormously if we can approximate the distributions as Gaussian, and this approximation is well supported by the data (*SI Appendix*, section D). The result for a single gene is then

$$\Delta I = \frac{1}{2}\langle \log_2[\sigma_g^2(x_s)]\rangle_{x_s} - \frac{1}{2}\langle \log_2[\sigma_g^2(x_s|L)]\rangle_{x_s,L}, \qquad [14]$$

where $\sigma_g^2(x_s|L)$ is the variance in concentration at scaled position x_s across embryos of length L and $\sigma_g^2(x_s)$ is the same variance computed across all embryos.

Applying Eq. **14** requires estimating the relevant variances and also making bins along the x_s and L axes. For the scaled position, we choose bins of size $\Delta x_s = 0.01$, consistent with the precision that we see in Figs. 1 and 2. To sample the range of embryo lengths we use $N_{\mathrm{bins}} = 5$, 10, 15, or 20 adaptive bins, and find the same results in all cases (*SI Appendix*, section E). As is well known, estimates of entropy or information are subject to systematic errors (43, 58). In the present case, if we substitute estimates of the variances into Eq. **14**, we find a nonzero result for ΔI. But suppose we include different numbers of embryos in our analysis. In that case, we see that our estimate of ΔI depends on $1/N_{\mathrm{em}}$ as expected theoretically (43, 58), and having seen this predicted dependence, we can extrapolate $N_{\mathrm{em}} \to \infty$. In particular, if we shuffle the data so that the true $\Delta I = 0$, then our estimation procedure returns a random number with zero mean and SD equal to our quoted error bar, demonstrating that we have control over the systematic errors. These now standard analysis methods are reviewed in *SI Appendix*, section E.

Results of this analysis for Hb are shown in Fig. 4*A*. Using all $N_{\mathrm{em}} = 301$ embryos in our dataset produces a very small estimate of ΔI, but even this is exaggerated by systematic errors as we see by changing N_{em}. Our best estimate extrapolates to zero as $N_{\mathrm{em}} \to \infty$, with an error bar smaller than 0.01 bits. When we repeat the same analyses for each of the other gap genes (i.e., Gt, Kni, and Kr), we get the same result (*SI Appendix*, section E and Fig. S8).

We can generalize this analysis to consider all four gap genes simultaneously. Now the role of the variance in Eq. **14** is played by the covariance matrix Σ of the fluctuations,

$$\Delta I = \frac{1}{2}\langle \log_2[||\Sigma(x_s)||]\rangle_{x_s} - \frac{1}{2}\langle \log_2[||\Sigma(x_s|L)||]\rangle_{x_s,L}. \qquad [15]$$

Here $||\Sigma(x_s|L)||$ is the determinant of the covariance matrix describing fluctuations in the expression levels of all four genes at scaled position x_s across embryos of length L, and $\Sigma(x_s|L)$ is the covariance computed across all embryos. Because we are looking at higher dimensional variations, the impact of the finiteness of our dataset is larger, but again, we see the predicted dependence on $1/N_{\mathrm{em}}$ and can extrapolate to give $\Delta I = 0.038 \pm 0.039$ bits (Fig. 4*B*). Once again this is consistent with $\Delta I = 0$: There is no significant evidence for encoding of information about absolute, as opposed to scaled position.

Although the number of bits has meaning, it is useful to express the deviation from perfect scaling as a fraction of the information available about scaled position (52, 57),

$$\frac{I(\mathbf{g} \to \{x, L\}) - I(\mathbf{g} \to x/L)}{I(\mathbf{g} \to x/L)} = 0.009 \pm 0.009. \qquad [16]$$

Thus gap gene expression patterns exhibit perfect scaling within experimental error, and the upper bound of this error is less than 2%. We emphasize that this is a statement not just about positional markers but about the entire range of graded spatial variations.

Maternal Inputs Are Not Scale Invariant

Having observed scaling in the pair-rule stripe positions and followed this back to the gap genes, it is natural to ask whether we can trace the scaling behavior of the patterning system to the maternal inputs. Among the three maternal gene systems that

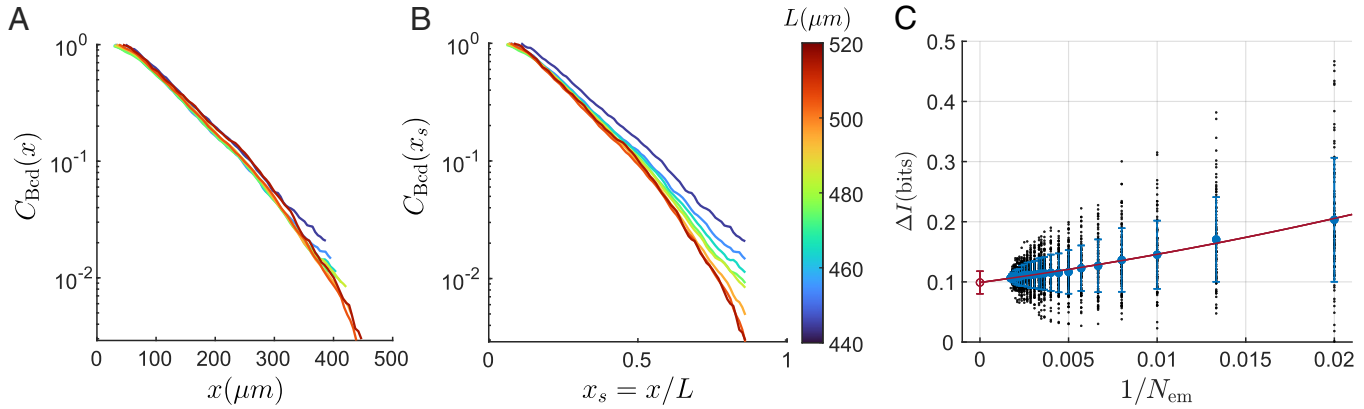

Fig. 5. The maternal morphogen Bcd does not scale with embryo size. (*A*) Measurements of Bcd concentration in $N_{\rm em} = 582$ live embryos are grouped into eight classes by embryo length L and averaged. There is only one global normalization, so this shows that absolute concentrations have the same dependence on absolute position x across all classes. (*B*) The same data plotted vs. scaled position $x_S = x/L$. Profiles separate, providing evidence against scaling. (*C*) Extra information ΔI that Bcd concentration provides about absolute vs. scaled position, defined by Eq. **10** and evaluated from Eq. **14**. Symbols as in Fig. 4, but the extrapolation now leads to a significantly nonzero value of $\Delta I = 0.1 \pm 0.02$ bits. Data from ref. 53.

drive patterning along the AP axis of the fly embryo (anterior, posterior, and terminal), much attention has been given to the principal anterior morphogen Bcd (28, 29). The protein is at high concentration in the anterior, and there is a nearly exponential decay of concentration with distance toward the posterior; one can monitor the dynamics of Bcd concentrations quantitatively in live embryos using fusions with the green fluorescent protein (37).

Comparison across several species of dipterans with different egg lengths (divergence in evolutionary time 50 to 60 mya) shows that the mean length scale of this exponential decay varies in proportion to the mean length of the embryo (1). However, previous work was inconclusive about whether the exponential decay is proportional to embryo length L within each population of the different species. This question has remained open partially because of the small fluctuations in L that occur naturally and demand very precise measurements. Insertion of *bcd* genes from other species into *Drosophila melanogaster* produces protein concentration profiles with length scales appropriate to the host, but these are not sufficient to rescue the embryo from deletion of the native Bcd (59). These results emphasize the subtlety of comparison across species and the impact of genetic variations, which lead us to reexamine the behavior of Bcd profiles across a large number of live embryos drawn from the same inbred laboratory strain used in the analysis of gap and pair-rule genes.

Fig. 5 analyzes Bcd profiles from $N_{\rm em} = 582$ live embryos (53). Measurements are taken during a small temporal window in nuclear cycle fourteen (37), and the only normalization (as with the gap genes) is to subtract a common background level from all the embryos and set the highest mean concentration to one. When we group the embryos into eight classes based on their length L, the average concentration profiles in all groups are the same when plotted vs. absolute position, except for small effects at the posterior pole (Fig. 5*A*). If we plot vs. scaled position, the different groups of embryos separate significantly (Fig. 5*B*), providing direct evidence *against* scaling.

The nearly exponential form of the Bcd profile, $C_{\rm Bcd}(x) \sim \exp(-x/\lambda)$, makes it tempting to test scaling by asking about the variation of the length scale λ with embryo length L. But the information-theoretic approach introduced above allows us to test for scaling—or the absence of scaling—in a way that does not depend on fitting a model. The result, in Fig. 5*C*, is that the positional information carried by Bcd has a significant nonzero value of $\Delta I = 0.1 \pm 0.02$ bits. While this may seem small, it corresponds to the ∼4% variation in embryo length. The conclusion is that the maternal morphogens do not scale, consistent with earlier suggestions (22).

We emphasize that the absence of scaling in the maternal morphogen Bcd should not in any sense be interpreted as noise. Indeed, absolute concentrations of Bcd protein are highly reproducible across embryos and this can be traced to highly reproducible numbers of mRNA molecules (53, 60, 61). Instead, we should think of Bcd as a nearly deterministic response to the embryo's boundary conditions, which impact the gap genes directly (*SI Appendix*, section F).

Scaling and Zero Modes

Scale invariance is a statement about the patterns of gene expression in space. Nonetheless, our findings on gap gene scaling have significant implications for network dynamics over time. To derive these implications, it is useful to think in terms of a broad class of models for the network dynamics.

There is a tension between building models that give a realistic description of one particular network and models that have some degree of generality. We will try for generality, including essential ingredients: Proteins diffuse and are degraded, and their synthesis is controlled—perhaps in complicated ways—by the concentrations of other proteins. To simplify we ignore the discreteness of the nuclei and describe the concentrations as varying continuously in space, as in the analysis of data above. To begin we also neglect noise, although we return to this below. Then a general model is

$$\tau_i \frac{\partial g_i}{\partial t} = \ell_i^2 \frac{\partial^2 g_i}{\partial x^2} + F_i(\mathbf{g}) - g_i. \qquad [17]$$

Here g_i is the concentration of the protein encoded by gene i, and τ_i is that protein's lifetime against degradation. The length scale $\ell_i = \sqrt{D_i \tau_i}$ is determined by the diffusion constants D_i and lifetimes. All of the complexity of molecular interactions is contained in the regulation functions $F_i(\mathbf{g})$, which describe how the rate of synthesis of the protein encoded by gene i depends on all the concentrations $\mathbf{g} = \{g_1, g_2, g_3, g_4\}$. We emphasize that $F_i(\mathbf{g})$ could encompass both activating and repressive interactions, potentially combinatorially. This set of

equations offers a very general description without microscopic details and includes Turing's original models (15) and their intellectual descendants (16, 62) as special cases. Eq. **17** looks like a model for an autonomous set of gap genes, but we will see below how to include the maternal inputs. More details are discussed in *SI Appendix*, section F.

It is important that the embryo length L does not appear directly in Eq. **17** describing the dynamics of the genetic network. The length appears instead only through boundary conditions. In the absence of sources or sinks, the concentration profiles must be such that there is no diffusive flux at either end of the embryo, which means that

$$D_i \frac{\partial g_i(x)}{\partial x}\bigg|_{x=0} = D_i \frac{\partial g_i(x)}{\partial x}\bigg|_{x=L} = 0. \quad [18]$$

Somehow these conditions at the ends of the embryo need to propagate into the interior to make the solutions of these equations scale-invariant.

Let us assume that the patterns we see are in steady state so that $g_i(x,t) = g_i(x)$, and scale invariance means that $g_i(x) = \hat{g}_i(x/L)$. Thus if we change the length of the embryo by a small amount δL, then the profiles of gene expression change

$$g_i(x) \to g_i(x) - \frac{\delta L}{L}\left[\frac{x}{L}\hat{g}_i'(x/L)\right], \quad [19]$$

where the prime denotes the derivative with respect to x/L. But this is just one way in which the profiles could change, and it is useful to think about some larger set of possibilities

$$g_i(x) \to g_i(x) - \sum_\mu a_\mu \phi_i^\mu(x). \quad [20]$$

The functions $\{\phi_i^\mu(x)\}$ are "modes" of variation in the expression profiles, and the amplitudes $\{a_\mu\}$ provide a coordinate system in this space of variations. Suppose we want to describe all the possibilities. Then the number of modes must be the number of genes times the number of independent points along the x axis, e.g. the number of rows of cells; for the gap genes, the result is that the space has a dimensionality $d > 300$.

One way of defining the modes $\{\phi_i^\mu(x)\}$ is to look at the profiles across a very large set of embryos and perform a principal components analysis (PCA). PCA chooses a set of modes such that the smallest number of modes captures as much of the total variance as possible, and the amplitudes of variation a_μ are (linearly) independent of one another.

The dynamics of the network also define a privileged set of modes. Since all the modes taken together describe all possible variations, we can describe time-dependent profiles by letting the amplitudes a_μ become time-dependent,

$$g_i(x) \to g_i(x) - \sum_\mu a_\mu(t) \phi_i^\mu(x). \quad [21]$$

If all the amplitudes are small, so that the system is close to its steady state, then the nonlinear Eq. **17** become linear in the $a_\mu(t)$. Further, if we choose the modes correctly the equations for the many amplitudes become independent of one another, and take the simple form

$$\frac{da_\mu(t)}{dt} = -\lambda_\mu a_\mu(t). \quad [22]$$

This means that as one gets close to the steady state the amplitude of variation along each mode decays exponentially at a rate λ_μ, independent of all the other modes. This simplification works only if we choose the modes to obey

$$\sum_j \left[\left(\ell_i^2 \frac{\partial^2}{\partial x^2} - 1\right)\delta_{ij} + \frac{\partial F_i}{\partial g_j}\bigg|_{\mathbf{g}=\hat{\mathbf{g}}}\right]\phi_j^\mu(x) = -\lambda_\mu \phi_i^\mu(x). \quad [23]$$

Formally, the dynamical modes are eigenfunctions of some linear operator. This is similar to the fact that principal components are eigenvectors of the covariance matrix of fluctuations around the mean. The condition in Eq. **23** is complicated; the surprise is that there is a connection to scale invariance.

To have scale invariance, the spatial profiles of gene expression still have to be steady-state solutions of the dynamical Eq. **17** for the network even after the transformation in Eq. **19**. For small δL this condition becomes *SI Appendix*, Eq. **S.52** in *SI Appendix*, section F,

$$\sum_j \left[\left(\ell_i^2 \frac{\partial^2}{\partial x^2} - 1\right)\delta_{ij} + \frac{\partial F_i}{\partial g_j}\bigg|_{\mathbf{g}=\hat{\mathbf{g}}}\right]\left[\frac{x}{L}\hat{g}_j'(x/L)\right] = 0. \quad [24]$$

We see that the linear operator that appears here is the same as the one that appears in Eq. **23**. This leads to two conclusions. First, how gene expression profiles transform as we change the length of the embryo has to be one of the natural dynamical modes of the network. Second, this mode has to be very special, with $\lambda_0 = 0$; such modes are called "zero modes."

In many physics problems, zero modes are guaranteed by some underlying symmetry (63). Although the analogies are imperfect, here the symmetry is scale invariance. The existence of a zero mode is a statement about the linearized dynamics. If the absence of a linear restoring force continues for finite deviations from the steady state then there is a line of attracting spatial patterns rather than a single stable pattern. Different points along this line are the patterns appropriate to embryos of different lengths, and boundary conditions select the final pattern. Line attractors have long been discussed for neural networks (64). It has been noted that models of the gap gene network might support such line attractors (33), and there are also suggestions that internal dynamics of the network can generate approximate scaling (34).

The existence of a zero mode in the network dynamics has several implications (see *SI Appendix*, section F for details):

- Most literally, one component in the spatial pattern of gene expression will relax very slowly to its steady state. Formally the relaxation will be as a power of time rather than exponential.
- The dynamics describe a "restoring force" that pulls gene expression patterns toward their steady state; the eigenvalues are the spring constants associated with these forces. There is no (linear) restoring force along the zero mode, and in the presence of noise, the fluctuations along this mode will be very large compared with other modes. This one dominant mode generates long-ranged spatial correlations among the fluctuations in gene expression.
- Along directions with nonzero λ_μ the fluctuations in $\mathbf{g}$ will be approximately Gaussian so long as they remain small, as we see for the gap genes. But along the zero mode, there should be some deviation from Gaussian behavior.

There are hints of all these effects in previous work (31, 32). Independent analyses indicate that the gap gene dynamics are dominated by a small number of modes (65), and other

arguments connect dynamics to scaling (66). More work is needed to see whether all these results fit into a coherent picture.

Finally, the model we have considered describes an autonomous network of gap genes. But maternal inputs such as Bcd are thought to obey similar equations, describing diffusion and degradation but no feedback regulating their synthesis, and with different boundary conditions, e.g. a source of Bcd at the anterior end of the embryo (37, 45, 67). Thus we can enlarge the class of models to include maternal inputs (*SI Appendix*, section F.E). In this larger system of equations, it remains true that scale invariance requires the existence of a zero mode. Since the zero mode emerges from interactions in a network, and Bcd feeds into the gap genes without any feedback, it is natural that maternal inputs do not scale. Related ideas appear in models where the gap gene network forms stable patterns independent of the maternal inputs, which then serve to anchor the pattern at the poles (68).

Discussion

Scale invariance is an appealing concept. It quantifies the intuition that organisms are built from parts in proportion to one another, independent of an individual organism's overall size. Here we have explored scaling across many embryos from a quasi-inbred laboratory stock of *D. melanogaster*, minimizing genetic variation. Across this ensemble, fluctuations in embryo length have a SD of 4%, with embryos in the tails of the distribution deviating ±10% from the mean (*SI Appendix*, Fig. S1). Following previous work, we measured the positions of discrete markers—the CF position, the peaks of pair-rule stripes, and the boundaries of gap gene domains—and found scaling of the absolute positions with embryo length. While consistent with previous results, we observe extreme precision: Markers are at positions scaled in proportion to the embryo length with an accuracy of ∼1% across the AP axis. This precision excludes a broad class of models that combine information from both ends of the embryo without explicit scaling (44–47).

There is a conceptual difference between scaling in the positioning of discrete markers and true, mathematical scale invariance of the patterns in gene expression. We have introduced an information-theoretic approach that analyzes the full, graded spatial profiles of expression and measures similarity in the natural units provided by the intrinsic noise levels of these profiles. Concretely, we introduce a decomposition of the information that morphogen concentrations provide about position into a component about the scaled position and a deviation from scaling. Applied to the gap genes in the early fly embryo, the result is clear: The deviation from scaling is less than two percent of the total positional information.

Our results build on a generation of work searching for scaling in the fly embryo. This has involved measuring the patterns of gene expression in *D. melanogaster* (22, 23, 25), comparing related species (1, 59), and evolving new lines of flies artificially selected for egg length (26, 69). By now the idea of scaling is not surprising. What is surprising is the precision of our result. In particular, *all* of the information gap gene expression levels provide about position along the AP axis is information about the scaled position, and "all" means more than 98%. Scaling emerges not just as some approximate compensation for changes in the length of the embryo, but rather as a precise mathematical statement of invariance.

Mathematically, robustness is the ability of a system to maintain certain behaviors despite variations in parameters defining the dynamics. In this way, we can think of scaling as a robustness of pattern formation to variations in egg length. This should not be taken as evidence for a general notion of robustness. As a counterexample, there is no need for robustness against variations in the concentration of maternal inputs, since these already are highly reproducible (60, 61).

The precise mathematical statement of scale invariance predicts that the dynamics of the underlying genetic network have a zero mode. These dynamics then do not have a single attractor but rather a line of attractors as in models for short-term memory in neural networks (64), and the zero mode corresponds to variations in the pattern of gene expression along this line in the high dimensional space of possible patterns. In a single embryo, position along the line of attractors is chosen by the boundary conditions and hence the length of the embryo. A zero mode connects otherwise disparate observations on gap gene expression patterns (31, 32).

In contrast to the results for the gap and pair-rule genes, at least one of the maternal determinants, Bcd, does not exhibit scaling. We can see this "by eye," simply plotting profiles vs. absolute or scaled position, and these impressions are quantified by the same information theoretic approaches used to demonstrate scaling in the gap genes. Error bars again are in the range of ∼0.01 bits, but the deviation from scaling now is 10× as large. The conclusion is that scale invariance is an emergent property of the gap gene network, and it seems plausible that the pair-rule genes then inherit this invariance. The argument that scaling results from zero modes predicts that Bcd profiles cannot scale since there is no feedback from other genes to Bcd (*SI Appendix*, section F). This means that the scaling of gap genes is possible even in the presence of nonscaling maternal morphogens. Our analysis does not include any assumptions about the cross-regulatory interactions among the gap genes. As such it does not provide a "mechanism" for the scale invariance of the gap genes, but rather provides general condition that such mechanisms, expressed as dynamical models, must obey. Additional work is needed to provide concrete examples that instantiate these general theoretical arguments.

Several results support the idea that scaling is an emergent property of the gap gene network. Previous work on the evolution of embryonic patterning across related *Drosophila* species has shown that traits (gene expression pattern boundary positions) can evolve without disrupting zygotic gene expression pattern reproducibility in scaled coordinates (25, 70). Other signs of emergent behavior appear in the gap gene network's dynamic response to varied Bcd concentrations (53) and in the rapid evolution of compensatory responses to these variations (71). However, the connection to scaling is not yet clear.

Scale invariance provides an anchor for thinking about positional information and genetic network function, especially in systems where not all the relevant components have been identified (72). Recent experiments on mammalian pseudoembryos suggest that scale invariance may be a more universal feature of genetic networks underlying developmental pattern formation (73). In these self-organizing aggregates derived from stem cells, scaling of gene expression patterns emerges spontaneously without externally imposed input or even fixed boundary conditions. The existence of such a different multicellular system that exhibits precise scaling makes the zero-mode networks an even more attractive scenario.

Data, Materials, and Software Availability. All data from refs. 40 and 53 used in this work, and the corresponding analysis code, is available at DOI: 10.5281/zenodo.13624094 (74).

ACKNOWLEDGMENTS. We thank U. Gerland, T. Ramalho, G. Reddy, T. Schupbach, and E.F. Wieschaus for advice and inspiring discussions. We also thank the four reviewers for their thorough reading of our manuscript and incisive comments. This work was supported in part by US NSF Grant PHY-1734030 (Center for the Physics of Biological Function); by NIH Grants R01GM077599 and R01GM097275; by the Simons Foundation; by the John Simon Guggenheim Memorial Foundation.

Author affiliations: [a]Joseph Henry Laboratories of Physics, Princeton University, Princeton, NJ 08544; [b]Lewis–Sigler Institute for Integrative Genomics, Princeton University, Princeton, NJ 08544; [c]Department of Physics, Lehman College, City University of New York, Bronx, NY 10468; [d]Key Laboratory of Hebei Province for Molecular Biophysics, Institute of Biophysics, School of Health Science and Biomedical Engineering, Hebei University of Technology, Tianjin 300130, China; [e]Program in Biophysics, Harvard University, Cambridge, MA 02138; [f]Initiative for the Theoretical Sciences, The Graduate Center, City University of New York, New York, NY 10016; and [g]Department of Developmental and Stem Cell Biology, CNRS UMR3738 Paris Cité, Institut Pasteur, Paris 75015, France

1. T. Gregor, W. Bialek, R. R. de Ruyter van Steveninck, D. W Tank, E. F. Wieschaus, Diffusion and scaling during early embryonic pattern formation. *Proc. Natl. Acad. Sci. U.S.A.* **102**, 18403–18407 (2005).
2. K. Ishimatsu *et al*., Size-reduced embryos reveal a gradient scaling based mechanism for zebrafish somite formation. *Development* **145**, dev161257 (2018).
3. M. Almuedo-Castillo *et al*., Scale-invariant patterning by size-dependent inhibition of nodal signalling. *Nat. Cell Biol.* **20**, 1032–1042 (2018).
4. A. Leibovich, T. Edri, S. L. Klein, S. A. Moody, A. Fainsod, Natural size variation among embryos leads to the corresponding scaling in gene expression. *Dev. Biol.* **462**, 165–179 (2020).
5. J. S. Huxley, *Problems of Relative Growth* (Meuthen, London, 1932).
6. T. A. McMahon, J. T. Bonner, *On Size and Life* (Scientific American Library, New York, 1983).
7. G. B. West, J. H. Brown, B. J. Enquist, A general model for the origin of allometric scaling laws in biology. *Science* **276**, 122–126 (1997).
8. J. Kepler, *The Six-Cornered Snowflake: A New Year's Gift* (Paul Dry Books, Philadelphia, PA, 2010).
9. K. G. Libbrecht, The physics of snow crystals. *Rep. Prog. Phys.* **68**, 855 (2005).
10. J. S. Langer, Instabilities and pattern formation in crystal growth. *Rev. Mod. Phys.* **52**, 1 (1980).
11. J. M. Flesselles, A. J. Simon, A. J. Libchaber, Dynamics of one-dimensional interfaces: An experimentalist's view. *Adv. Phys.* **40**, 1–51 (1991).
12. M. C. Cross, P. C. Hohenberg, Pattern formation outside of equilibrium. *Rev. Mod. Phys.* **65**, 851 (1993).
13. M. Lappa, *Thermal Convection: Patterns, Evolution and Stability* (John Wiley and Sons, New York, 2009).
14. J. S. Langer, Dendrites, viscous fingers, and the theory of pattern formation. *Science* **243**, 1150 (1989).
15. A. M. Turing, The chemical basis of morphogenesis. *Philos. Trans. R. Soc. Lond. B* **237**, 37–71 (1952).
16. A. Gierer, H. Meinhardt, A theory of biological pattern formation. *Kybernetik* **12**, 30–39 (1972).
17. R. Phillips, J. Kondev, J. Theriot, H. Garcia, *Physical Biology of the Cell* (Garland Science, 2012).
18. J. Raspopovic, L. Marcon, L. Russo, J. Sharpe, Digit patterning is controlled by a bmp-sox9-wnt turing network modulated by morphogen gradients. *Science* **345**, 566–570 (2014).
19. M. P. Scott, S. B. Carroll, The segmentation and homeotic gene network in early *Drosophila* development. *Cell* **51**, P689–698 (1987).
20. J. Jaeger, B. Verd, Dynamic positional information: Patterning mechanism versus precision in gradient-driven systems. *Curr. Top. Dev. Biol.* **137**, 219–246 (2020).
21. G. Tkačik, T. Gregor, The many bits of positional information. *Development* **148**, dev176065 (2021).
22. B. Houchmandzadeh, E. Wieschaus, S. Leibler, Establishment of developmental precision and proportions in the early *Drosophila* embryo. *Nature* **415**, 798–802 (2002).
23. S. Surkova *et al*., Characterization of the *Drosophila* segment determination morphome. *Dev. Biol.* **313**, 844–862 (2008).
24. D. M. Holloway, L. G. Harrison, D. Kosman, C. E. Vanario-Alonso, A. V. Spirov, Analysis of pattern precision shows that drosophila segmentation develops substantial independence from gradients of maternal gene products. *Dev. Dyn.* **235**, 2949–2960 (2006).
25. S. E. Lott, M. Kreitman, A. Palsson, E. Alekseeva, M. Z. Ludwig, Canalization of segmentation and its evolution in *Drosophila*. *Proc. Natl. Acad. Sci. U.S.A.* **104**, 10926–10931 (2007).
26. C. M. Miles *et al*., Artificial selection on egg size perturbs early pattern formation in *Drosophila melanogaster*. *Evolution* **65**, 33–42 (2011).
27. V. Antonetti *et al*., Precise spatial scaling in the early fly embryo. arXiv [Preprint] (2018). https://arxiv.org/abs/1812.11384 (Accessed 15 February 2024).
28. W. Driever, C. Nüsslein-Volhard, A gradient of bicoid protein in *Drosophila* embryos. *Cell* **54**, 83–93 (1988).
29. W. Driever, C. Nüsslein-Volhard, The bicoid protein determines position in the *Drosophila* embryo in a concentration-dependent manner. *Cell* **54**, 95–104 (1988).
30. D. Cheung, C. Miles, M. Kreitman, J. Ma, Scaling of the Bicoid morphogen gradient by a volume-dependent production rate. *Development* **138**, 2741–2749 (2011).
31. D. Krotov, J. O. Dubuis, T. Gregor, W. Bialek, Morphogenesis at criticality. *Proc. Natl. Acad. Sci. U.S.A.* **111**, 3683–3688 (2014).
32. L. McGough *et al*., Finding the last bits of positional information. *PRX Life* **2**, 013016 (2024).
33. Manu, *et al*., Canalization of gene expression and domain shifts in the *Drosophila* blastoderm by dynamical attractors. *PLoS Comput. Biol.* **5**, e1000303 (2009).
34. S. Vakulenko, M. J. Reinitz, O. Radulescu, Size regulation in the segmentation of *Drosophila*: Interacting interfaces between localized domains of gene expression ensure robust spatial patterning. *Phys. Rev. Lett.* **103**, 168102 (2009).
35. L. Wolpert, Positional information and the spatial pattern of cellular differentiation. *J. Theor. Biol.* **25**, 1–47 (1969).
36. P. A. Lawrence, *The Making of a Fly: The Genetics of Animal Design* (Blackwell Scientific Publications Ltd., Oxford, 1992).
37. T. Gregor, E. F. Wieschaus, A. P. McGregor, W. Bialek, D. W. Tank, Stability and nuclear dynamics of the bicoid morphogen gradient. *Cell* **130**, 141–152 (2007).
38. E. M. Smith, "Scaling and regulation of gene expression in the developing fly embryo," Ph.D. thesis, Princeton University (2015).
39. J. O. Dubuis, R. Samanta, T. Gregor, Accurate measurements of dynamics and reproducibility in small genetic networks. *Mol. Syst. Biol.* **9**, 639 (2013).
40. M. D. Petkova, G. Tkačik, W. Bialek, E. F. Wieschaus, T. Gregor, Optimal decoding of cellular identities in a genetic network. *Cell* **176**, 844–855 (2019).
41. C. E. Shannon, A mathematical theory of communication. *Bell Syst. Tech. J.* **27**, 379–423 (1948).
42. T. M. Cover, J. A. Thomas, *Elements of Information Theory* (Wiley and Sons, New York, 1991).
43. W. Bialek, *Biophysics: Searching for Principles* (Princeton University Press, 2012).
44. M. Howard, P. R. ten Wolde, Finding the center reliably: Robust patterns of developmental gene expression. *Phys. Rev. Lett.* **95**, 208103 (2005).
45. B. Houchmandzadeh, E. Wieschaus, S. Leibler, Precise domain specification in the developing *Drosophila* embryo. *Phys. Rev. E* **72**, 061920 (2005).
46. P. McHale, W. J. Rappel, H. Levine, Embryonic pattern scaling achieved by oppositely directed morphogen gradients. *Phys. Biol.* **3**, 107 (2006).
47. D. Čapek, P. Müller, Positional information and tissue scaling during development and regeneration. *Development* **146**, dev177709 (2019).
48. M. Frasch, R. Warrior, J. Tugwood, M. Levine, Molecular analysis of even-skipped mutants in *Drosophila* development. *Genes Dev.* **2**, 1824–1838 (1988).
49. J. Jaeger *et al*., Dynamic control of positional information in the early *Drosophila* embryo. *Nature* **430**, 368–371 (2004).
50. J. Jaeger *et al*., Dynamical analysis of regulatory interactions in the gap gene system of *Drosophila melanogaster*. *Genetics* **167**, 1721–1737 (2004).
51. J. P. Bothma *et al*., Dynamic regulation of eve stripe 2 expression reveals transcriptional bursts in living *Drosophila* embryos. *Proc. Natl. Acad. Sci. U.S.A.* **111**, 10598–10603 (2014).
52. J. O. Dubuis, G. Tkačik, E. F. Wieschaus, T. Gregor, W. Bialek, Positional information, in bits. *Proc. Natl. Acad. Sci. U.S.A.* **110**, 16301–16308 (2013).
53. F. Liu, A. H. Morrison, T. Gregor, Dynamic interpretation of maternal inputs by the *Drosophila* segmentation gene network. *Proc. Natl. Acad. Sci. U.S.A.* **110**, 6724–6729 (2013).
54. A. Vincent, J. T. Blankenship, E. Wieschaus, Integration of the head and trunk segmentation systems controls cephalic furrow formation in *Drosophila*. *Development* **124**, 3747–3754 (1997).
55. J. Jaeger, The gap gene network. *Cell. Mol. Life Sci.* **68**, 243–274 (2011).
56. R. Warrior, M. Levine, Dose-dependent regulation of pair-rule stripes by gap proteins and the initiation of segment polarity. *Development* **110**, 759–767 (1990).
57. G. Tkačik, J. O. Dubuis, M. D. Petkova, T. Gregor, Positional information, positional error, and readout precision in morphogenesis: A mathematical framework. *Genetics* **199**, 39–59 (2015).
58. G. Miller, "Note on the bias of information estimates in Information Theory" in *Psychology II-B: Problems and Methods*, H. Quastler, Ed. (Free Press, Glencoe IL, 1955), pp. 95–100.
59. T. Gregor, A. P. McGregor, E. F. Wieschaus, Shape and function of the bicoid morphogen gradient in dipteran species with different sized embryos. *Dev. Biol.* **316**, 350–358 (2008).
60. T. Gregor, D. W. Tank, E. F. Wieschaus, W. Bialek, Probing the limits to positional information. *Cell* **130**, 153–164 (2007).
61. M. D. Petkova, S. C. Little, F. Liu, T. Gregor, Maternal origins of developmental reproducibility. *Curr. Biol.* **24**, 1283–1288 (2014).
62. H. Meinhardt, Models of biological pattern formation: From elementary steps to the organization of embryonic axes. *Curr. Top. Dev. Biol.* **81**, 1–63 (2008).
63. P. M. Chaikin, T. C. Lubensky, *Principles of Condensed Matter Physics* (Cambridge University Press, Cambridge, 1995).
64. H. S. Seung, How the brain keeps the eyes still. *Proc. Natl. Acad. Sci. U.S.A.* **93**, 13334–13339 (1996).
65. R. Seyboldt *et al*., Latent space of a small genetic network: Geometry of dynamics and information. *Proc. Natl. Acad. Sci. U.S.A.* **119**, e2113651119 (2022).
66. J. Shen, F. Liu, C. Tang, Scaling dictates the decoder structure. *Sci. Bull.* **67**, 1486–1495 (2022).
67. O. Grimm, M. Coppey, E. Wieschaus, Modelling the bicoid gradient. *Development* **137**, 2253–2264 (2010).
68. M. Majka, N. B. Becker, P. R. ten Wolde, M. Zagorski, T. R. Sokolowski, Stable developmental patterns of gene expression without morphogen gradients. arXiv [Preprint] (2023). https://arxiv.org/abs/2306.00537 (Accessed 15 February 2024).
69. R. Xu *et al*., Shaping the scaling characteristics of gap gene expression patterns in *Drosophila*. *Heliyon* **9**, e13623 (2023).
70. S. E. Lott, M. Z. Ludwig, M. Kreitman, Evolution and inheritance of early embryonic patterning in *Drosophila simulans* and *D. sechellia*. *Evolution* **65**, 1388–1399 (2011).
71. X. C. Li *et al*., Rapid response of fly populations to gene dosage across development and generations. *Nat. Commun.* **15**, 4551 (2024).
72. M. Zagorski *et al*., Decoding of position in the developing neural tube from antiparallel morphogen gradients. *Science* **356**, 1379–1383 (2017).
73. M. Merle, L. Friedman, C. Chureau, A. Shoushtarizadeh, T. Gregor, Precise and scalable self-organization in mammalian pseudo-embryos. *Nat. Struct. Mol. Biol.* **31**, 896–902 (2024).
74. M. Nikolić *et al*., Scale invariance in early embryonic development. Zenodo. https://zenodo.org/records/13624094. Deposited 25 September 2024.